O. Barry[1]
Department of Mechanical
and Industrial Engineering,
University of Toronto,
Toronto, ON M5S 3G8, Canada
e-mail: oumar.barry@utoronto.ca

J. W. Zu
Department of Mechanical
and Industrial Engineering,
University of Toronto,
Toronto, ON M5S 3G8, Canada

D. C. D. Oguamanam
Department of Mechanical
and Industrial Engineering,
Ryerson University,
Toronto, ON M5B 2K3, Canada

Nonlinear Dynamics of Stockbridge Dampers

The present paper deals with the nonlinear dynamics of a Stockbridge damper. The nonlinearity is from damping and the geometric stretching of the messenger. The Stockbridge damper is modeled as two cantilevered beams with tip masses. The equations of motion and boundary conditions are derived using Hamilton's principle. The model is valid for both symmetric and asymmetric Stockbridge dampers. Explicit expressions are presented for the frequency equation, mode shapes, nonlinear frequency, and modulation equations. Experiments are conducted to validate the proposed model. [DOI: 10.1115/1.4029526]

Keywords: Stockbridge damper, Strouhal frequency, messenger

1 Introduction

Stockbridge dampers are the most common devices used to control aeolian vibration of overhead power lines. They eliminate or reduce the vibration level of the conductor by absorbing the wind energy. This absorption of the wind energy is only possible when their natural frequencies are tuned to cover the range of the forcing frequency, which is also known as Strouhal frequency. The modern Stockbridge damper has two types of dampers, namely, 2R damper and 4R damper [1]. The former, 2R damper, is a symmetric damper consisting of two identical weights and messengers at both ends. It has two natural modes of vibration. The latter, 4R damper, is an asymmetric damper and is depicted in Fig. 1. It is made-up of unequal weights and unequal messenger lengths on each side. This type of Stockbridge damper exhibits up to four resonant frequencies.

The damping mechanism of the Stockbridge damper is based on the transfer of vibrations of the conductor through the clamp to the messenger cable. The flexing of the messenger causes slipping between its strands which induces oscillation in the weights at their ends.

Several authors have examined the dynamics of the Stockbridge damper. The common approach is to experimentally determine its impedance curve [2–10]. Another approach is to model the Stockbridge damper as a two degree-of-freedom system [11,12].

An attempt to depart from the conventional way of modeling the Stockbridge damper was reported in Refs. [13–16]. The messenger cable was modeled as an Euler–Bernoulli beam and the counterweight was modeled as mass with a rotatory inertia. Both studies omitted the geometric nonlinearity of the messenger cable and employed the finite element method.

The current study presents an analytical model that accounts for the nonlinearity of the messenger cable. Numerous authors (see Refs. [17–24]) have examined the nonlinear vibration of beams with attached mass or spring mass. However, these investigations are limited to cases with end support. In the present study, the support is in-span and a tip mass is attached at each end. Hamilton's principle is used to derive the system governing equations. Explicit expressions are presented for the frequency modulation equations, mode shapes, and the nonlinear natural frequency. Experiments are conducted using three different Stockbridge dampers to benchmark the analytical model. Parametric studies are then performed to examine the effect of the damper parameters on the natural frequency and response.

2 Description of the System

A schematic of a single conductor with a Stockbridge damper is depicted in Fig. 1. It consists of a clamp, a messenger (or damper cable), and a mass (or counterweight) at each end of the messenger. The system of messenger and damper counterweights are modeled as two cantilevered Euler–Bernoulli beams with tip masses, as shown in Fig. 2. The attachment is the clamp which is interpreted as an infinitely rigid body.

3 Equations of Motion

A reference frame is attached to the clamp as shown in Fig. 2. The system kinetic and potential energies are given as

$$T = \sum_{j=1}^{2} \left(\frac{1}{2} m \int_0^{L_j} \dot{w}_j^2 dx + \frac{1}{2} M_j \dot{w}_j^2(L_j, t) + \frac{1}{2} J_j \dot{w}_j'^2 \right) \tag{1}$$

$$V = \sum_{j=1}^{2} \left(\frac{1}{2} EI \int_0^{L_j} w_j''^2 + \frac{1}{2} EA \int_0^{L_j} \left(u_j' + \frac{1}{2} w_j'^2 \right)^2 dx \right) \tag{2}$$

where E denotes the Young's modulus of elasticity of the messenger, I represents the moment of inertia of the messenger, A is the messenger cross section area, and m is the mass per unit length of the messenger. W_1 and W_2 denote the transverse displacement of the messenger on the left-hand side and right-hand side,

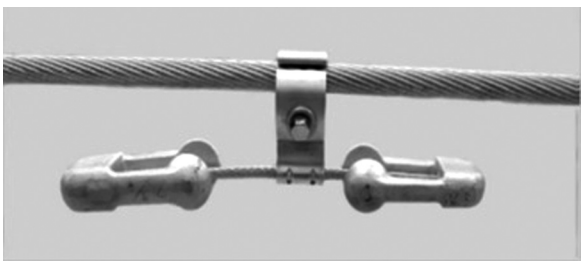

Fig. 1 Photograph of Stockbridge damper

[1]Corresponding author.

Contributed by the Dynamic Systems Division of ASME for publication in the Journal of Dynamic Systems, Measurement, and Control. Manuscript received September 7, 2013; final manuscript received December 29, 2014; published online February 9, 2015. Assoc. Editor: Jiong Tang.

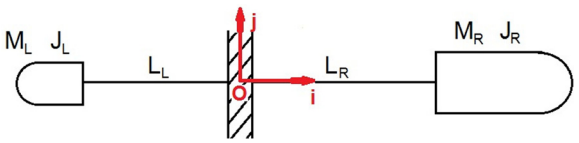

Fig. 2 Schematic of two cantilevered beams with tip masses

respectively. M_1 and M_2 are the mass of the left and right counterweights, respectively. J_1 and J_2 are the rotational inertia of left and right counterweights, respectively. L_1 and L_2 are the length of the left and right messengers, respectively. The primes and dots represent the derivative with respect to the axial coordinate x and time t, respectively.

Using Hamilton's principle and eliminating the axial displacement between Eqs. (1) and (2) yields the following equations of motion:

$$EIw_j'''' + m\ddot{w}_j = \frac{EA}{2L}\left[\sum_{i=1}^{2}\int_0^{L_i} {w_i'}^2 dx\right] w_j'' \tag{3}$$

and the accompanying boundary conditions are given as

$$w_1(0) = w_2(0) = w_1'(0) = w_2'(0) = 0 \tag{4}$$

$$EIw_j'''(L_j) = M_j\ddot{w}_j(L_j) \tag{5}$$

$$EIw_j''(L_j) = -J_j\ddot{w}_j'(L_j) \tag{6}$$

4 Free Vibration Analysis

The introduction of the following dimensionless parameters:

$$\tau = \frac{t}{L^2}\sqrt{\frac{EI}{m}}, \quad \zeta = \frac{x}{L}, \quad \xi_j = \frac{L_j}{L}, \quad W_j = \frac{w_j}{L}, \quad \alpha_j = \frac{M_j}{mL},$$
$$\gamma_j = \frac{J_j}{mL^3}, \quad f_n = \frac{FL^3}{EI}, \quad r = \sqrt{\frac{I}{AL^2}}, \quad \delta(\zeta) = \frac{\delta(x)}{L} \tag{7}$$

permits Eqs. (3)–(6) to be rewritten nondimensionally as

$$W_j'''' + \ddot{W}_j = \frac{1}{2}W_j''\left[\sum_{i=1}^{2}\int_0^{\xi_i} {W_i'}^2 d\zeta\right] \tag{8}$$

$$W_1(0) = W_2(0) = W_1'(0) = W_2'(0) = 0 \tag{9}$$

$$W_j'''(\xi_j) = \alpha_j\ddot{W}_j(\xi_j) \tag{10}$$

$$W_j''(\xi_j) = -\gamma_j\ddot{W}_j'(\xi_j) \tag{11}$$

The nondimensional displacement $W_j(\zeta,\tau)$ is expanded in the modal basis of the messenger Y_{jm} (i.e., the mode shape of a cantilevered beam with tip mass) as

$$W_j(\zeta,\tau) = r^k\sum_{m=1}^{N} q_m(\tau)Y_{jm}(\zeta) \tag{12}$$

where $Y_{jm}(\zeta)$ is the mth mode shape of the messenger and can be expressed as

$$Y_{jm}(\varsigma_j) = \left[\cos(\Omega\varsigma_j) - \lambda_j\sin(\Omega\varsigma_j) - \cos h(\Omega\varsigma_j) + \lambda_j\sin h(\Omega\varsigma_j)\right] \tag{13}$$

where

$$\lambda_j = \frac{(sh_1 + \alpha_j\Omega ch_j) - (s_j + \alpha_j\Omega c_i)}{(ch_j + \alpha_j\Omega sh_j) - (-c_j + \alpha_j\Omega s_j)}$$

and the following abbreviations are employed: $s_j = \sin\Omega\xi_j$, $c_j = \cos\Omega\xi_j$, $sh_j = \sin h\Omega\xi_j$, and $ch_j = \cos h\Omega\xi_j$.

The linear natural frequencies are the roots of the following frequency equation:

$$\prod_{j=1}^{2}[\gamma_j\alpha_j\Omega^4(c_jch_j - 1) + \gamma_j\Omega^3(s_jch_j + c_jch_j) + \alpha_j\Omega(s_jch_j - c_jsh_j) - 1 - c_jsh_j] = 0 \tag{14}$$

For the nonlinear problem, Eq. (12) is substituted into Eq. (8) to get

$$\sum_{m=1}^{N}(\ddot{q}_m + \omega_m^2 q_m)Y_{jm} = \frac{r^{2(k-1)}}{2}\left[\left(\sum_{m=1}^{N} q_m Y_{jm}''\right) \times \left(\sum_{p=1}^{N}\sum_{s=1}^{N} q_p q_s \sum_{j=1}^{2}\int_0^{\xi_j} Y_{jp}'Y_{js}'d\zeta\right)\right] \tag{15}$$

When Eq. (15) is explicitly written for $j=1$ and $j=2$, the resulting equations are correspondingly multiplied by Y_{n1} and Y_{n2}, the first expression is integrated over the range of 0 to ξ_1 and the second over 0 to ξ_2, then adding the two resulting equations as well as applying orthogonality and boundary conditions yields

$$\ddot{q}_n + \omega_n^2 q_n = \frac{r^{2(k-1)}}{2}\left[\left(\sum_{m=1}^{N} q_m \sum_{j=1}^{2}\int_0^{\xi_j} Y_{jm}''Y_{jn}d\zeta\right) \times \left(\sum_{p=1}^{N}\sum_{s=1}^{N} q_p q_s \sum_{j=1}^{2}\int_0^{\xi_j} Y_{jp}'Y_{js}'d\zeta\right)\right] \tag{16}$$

The right-hand side of Eq. (16) may be rewritten as

$$\Gamma_{mnps} = -\frac{1}{2}\sum_{j=1}^{2}\left(\int_0^{\xi_i} Y_{jm}'Y_{in}'d\zeta\right)\left(\int_0^{\xi_j} Y_{jp}'Y_{js}'d\zeta\right) \tag{17}$$

It is noted that Γ_{mnps} has both minor and major symmetries.

In order to obtain an approximate solution to Eq. (16), in cognizance of the accompanying boundary and initial conditions, the slenderness ratio r is, as is commonly the case in nonlinear beam vibration literature [18], identified as the parameter to define the degree of nonlinearity of the equations. Hence, the perturbation parameter, ϵ, depends on the slenderness ratio r and can be expressed as $\epsilon = r^{2(k-1)}$. If damping and forcing terms (μ_n and f_n) are added to Eq. (16), then

$$\ddot{q}_n + \omega_n^2 q_n = \epsilon\left[\sum_{m=1}^{N}\sum_{p=1}^{N}\sum_{s=1}^{N} q_m q_p q_s \Gamma_{mnps} - 2\mu_n\dot{q}_n\right] + f_n \tag{18}$$

For the special case of undamped free vibration, $\mu_n = 0$ and $f_n = 0$, Eq. (18) becomes

$$\ddot{q}_n + \omega_n^2 q_n = \epsilon\sum_{m=1}^{N}\sum_{p=1}^{N}\sum_{s=1}^{N} q_m q_p q_s \Gamma_{mnps} \tag{19}$$

This equation is solved using the multiple scales method, which is one of numerous available methods to obtain approximate solutions of nonlinear differential equations. The fundamental premise of the method is the uniform expansion of the dependent variable in terms of two or more independent variables which are commonly called scales. These scales are further distinguished as fast time or slow time. The former is the original independent variable, real time, and the latter is a function of the perturbation parameter

ϵ. References [18–24] can be consulted for detailed information on the method.

Using the multiple scales method to solve Eq. (19), q_n can be expressed in terms of ϵ such that

$$q_n = q_{n0} + \epsilon q_{n1} + O(\epsilon^2) \tag{20}$$

Let $T_0 = \tau, T_1 = \epsilon\tau, T_2 = \epsilon^2\tau$, and $T_n = \epsilon^n\tau$. T_0 and T_i ($i = 1, 2,..., n$) are called fast and slow time, respectively. The differential operator with respect to the time scale τ can be expanded to $O(\epsilon^2)$

$$\frac{d}{d\tau} = D_0 + \epsilon D_1, \quad \frac{d^2}{d\tau^2} = D_0^2 + 2\epsilon D_0 D_1 \tag{21}$$

where $D_0 = \partial/\partial T_0$ and $D_1 = \partial/\partial T_1$. Substituting Eqs. (21) and (20) into Eq. (19) yields

$$\begin{aligned}&\left(D_0^2 + 2\epsilon D_0 D_1\right)(q_{n0} + \epsilon q_{n1}) + \omega_n^2(q_{n0} + \epsilon q_{n1}) \\ &\quad = \epsilon \sum_{m=1}^{N}\sum_{p=1}^{N}\sum_{s=1}^{N} q_m q_p q_s \Gamma_{mnps}\end{aligned} \tag{22}$$

Collecting terms of the same order of ϵ yields

$$\text{order } \epsilon^0 : D_0^2 q_{n0} + \omega_n^2 q_{n0} = 0 \tag{23}$$

$$\begin{aligned}&\text{order } \epsilon^1 : D_0^2 q_{n1} + \omega_n^2 q_{n1} \\ &\quad = -2\epsilon D_0 D_1 q_{n0} + \sum_{m=1}^{N}\sum_{p=1}^{N}\sum_{s=1}^{N} q_m q_p q_s \Gamma_{mnps}\end{aligned} \tag{24}$$

The solution of Eq. (23) can be expressed as

$$q_{n0} = A_n(\tau_1)e^{i\omega_n\tau_0} + \text{cc} \tag{25}$$

where A_n is a complex function of slow time, ω_n is the linear natural frequency, and cc is the complex conjugate of the preceding terms. Substituting Eq. (25) into Eq. (24) yields

$$\begin{aligned}D_0^2 q_{n1} + \omega_n^2 q_{n1} &= -2i\omega_n D_1 A_n e^{i\omega_n\tau_0} \\ &\quad + \sum_{m=1}^{N}\sum_{p=1}^{N}\sum_{s=1}^{N} \Gamma_{mnps}\Big\{A_m A_p A_s e^{i(\omega_n+\omega_p+\omega_s)\tau_0} \\ &\quad + \bar{A}_m A_p A_s e^{i(-\omega_n+\omega_p+\omega_s)\tau_0} + A_m \bar{A}_p A_s e^{i(\omega_n-\omega_p+\omega_s)\tau_0} \\ &\quad + A_m A_p \bar{A}_s e^{i(\omega_n+\omega_p-\omega_s)\tau_0}\Big\} + \text{ccc}\end{aligned} \tag{26}$$

To obtain a periodic solution for Eq. (24), the secular terms in Eq. (26) must vanish. The secular term can be expressed as

$$-2i\omega_n A_n' + \sum_{m=1,n\neq m}^{N} A_m \bar{A}_m A_n(4\Gamma_{mnmn} + 2\Gamma_{mmnn}) + 3A_n^2\bar{A}_n\Gamma_{nnnn} = 0 \tag{27}$$

A_n can be expressed in the polar form as

$$A_n(\tau_1) = \frac{1}{2}a_n(\tau_1)e^{i\beta_n(\tau_1)} \tag{28}$$

Substituting Eq. (28) into Eq. (27) and separating real terms from imaginary terms yields

$$\omega_n a_n' = 0 \tag{29}$$

$$\omega_n a_n \beta_n' + \frac{1}{2}a_n \sum_{m=1,n\neq m}^{N} a_m^2\left(\Gamma_{mnmn} + \frac{1}{2}\Gamma_{mmnn}\right) + \frac{3}{8}a_n^3\Gamma_{nnnn} = 0 \tag{30}$$

From Eq. (29), $a_n' = 0$ yields

$$a_n = a_{n0} = \text{constant} \tag{31}$$

and Eq. (30) gives

$$\beta_n' = -\frac{1}{\omega_n}\left[\frac{1}{2}\sum_{m=1,n\neq m}^{N} a_m^2\left(\Gamma_{mnmn} + \frac{1}{2}\Gamma_{mmnn}\right) + \frac{3}{8}a_n^2\Gamma_{nnnn}\right] \tag{32}$$

The integration of Eq. (32) with respect to τ_1 and use of the relation $\tau_1 = \epsilon\tau_0$ yields

$$\beta_n = -\frac{\epsilon\tau_0}{\omega_n}\left[\frac{1}{2}\sum_{m=1,n\neq m}^{N} a_m^2\left(\Gamma_{mnmn} + \frac{1}{2}\Gamma_{mmnn}\right) + \frac{3}{8}a_n^2\Gamma_{nnnn}\right] + \beta_{n0} \tag{33}$$

The zero-order approximation can now be expressed as

$$\begin{aligned}q_{n0} = \frac{1}{2}a_{n0}e^{i\left[\omega_n - \frac{\epsilon}{\omega_n}\left\{\frac{1}{2}\sum_{m=1,n\neq m}^{N} a_{n0}^2\left(\Gamma_{mnmn} + \frac{1}{2}\Gamma_{mmnn}\right)\right.\right.} \\ \left.\left. + \frac{3}{8}a_{n0}^2\Gamma_{nnnn}\right\}\right]\tau_0 + i\beta_{n0} + \text{cc}\end{aligned} \tag{34}$$

while the nonlinear frequency is

$$\omega_{n,\text{NL}} = \omega_n - \frac{\epsilon}{\omega_n}\left(\frac{1}{2}\sum_{m=1,n\neq m}^{N} a_{m0}^2\left(\Gamma_{mnmn} + \frac{1}{2}\Gamma_{mmnn}\right) + \frac{3}{8}a_{n0}^2\Gamma_{nnnn}\right) \tag{35}$$

5 Forced Vibration

Consider primary resonance: $\Omega = \omega_1 + \epsilon\sigma$ where σ is a detuning parameter that quantitatively describes the nearest of Ω to ω_1. If the forcing term is expressed as $f_n = \epsilon f_0 e^{i\Omega t} + \text{cc}$, then Eq. (18) can be rewritten as

$$\ddot{q}_n + \omega_n^2 q_n = \epsilon\left[\sum_{m=1}^{N}\sum_{p=1}^{N}\sum_{s=1}^{N} q_m q_p q_s \Gamma_{mnps} - 2\mu_n\dot{q}_n\right] + 2\epsilon f_0 \sin\Omega t \tag{36}$$

$$f_n = \epsilon f_0 e^{i\Omega t} + \text{cc} \tag{37}$$

Equation (38) is easily deduced by following the procedure outlined in Sec. 4:

$$\begin{aligned}D_0^2 q_{n1} + \omega_n^2 q_{n1} &= -2i\omega_n D_1 A_n e^{i\omega_n\tau_0} - 2i\mu_n\omega_n A_n e^{i\omega_n\tau_0} + f_0 e^{i\Omega t} \\ &\quad + \sum_{m=1}^{N}\sum_{p=1}^{N}\sum_{s=1}^{N} \Gamma_{mnps}\Big\{A_m A_p A_s e^{i(\omega_n+\omega_p+\omega_s)\tau_0} \\ &\quad + \bar{A}_m A_p A_s e^{i(-\omega_n+\omega_p+\omega_s)\tau_0} + A_m \bar{A}_p A_s e^{i(\omega_n-\omega_p+\omega_s)\tau_0} \\ &\quad + A_m A_p \bar{A}_s e^{i(\omega_n+\omega_p-\omega_s)\tau_0}\Big\} + \text{ccc}\end{aligned} \tag{38}$$

The solvability condition that yields the elimination of the secular term can be expressed as

For $n = 1$

$$\begin{aligned}&-2i\omega_1\left(A_1' + \mu_1 A_1\right) + f_0 e^{i\sigma_1\tau_1} + A_1\sum_{m=2}^{N} A_m\bar{A}_m(4\Gamma_{m1m1} + 2\Gamma_{mm11}) \\ &\quad + 3A_1^2\bar{A}_1\Gamma_{1111} = 0\end{aligned} \tag{39}$$

For $n \geq 2$

$$-2i\omega_n\left(A_n' + \mu_n A_n\right) + A_n \sum_{m=1,n\neq m}^{N} A_m \bar{A}_m (4\Gamma_{mnmn} + 2\Gamma_{mmnn}) + 3A_n^2 \bar{A}_n \Gamma_{nnnn} = 0 \tag{40}$$

Using Eq. (28) in Eqs. (39) and (40) yields
For $n = 1$

$$-i\omega_1\left(a_1' + ia_1\beta_1' + \mu_1 a_1\right) + f_0 e^{i(\sigma_1\tau_1 - \beta_1)} + \frac{1}{2}a_1 \sum_{m=2}^{N} \frac{1}{4}a_m^2 (4\Gamma_{m1m1} + 2\Gamma_{mm11}) + \frac{3}{8}a_1^3\Gamma_{1111} = 0 \tag{41}$$

For $n \geq 2$

$$-i\omega_n\left(a_n' + ia_n\beta_n' + \mu_n a_n\right) + \frac{1}{2}a_n \sum_{m=1,n\neq m}^{N} \frac{1}{4}a_m^2 (4\Gamma_{mnmn} + 2\Gamma_{mmnn}) + \frac{3}{8}a_1^3\Gamma_{nnnn} = 0 \tag{42}$$

Collecting real terms and imaginary terms in Eq. (41) yields

$$-\omega_1(a_1' + \mu_1 a_1) + f_0 \sin(\sigma_1\tau_1 - \beta_1) = 0 \tag{43}$$

$$\omega_1 a_1\beta_1' + f_0\cos(\sigma_1\tau_1 - \beta_1) + \frac{1}{2}a_1 \sum_{m=2}^{N} \frac{1}{4}a_m^2 (4\Gamma_{m1m1} + 2\Gamma_{mm11}) + \frac{3}{8}a_1^3\Gamma_{1111} = 0 \tag{44}$$

and repeating the same for Eq. (42) yields

$$-\omega_n(a_n' + \mu_n a_n) + f_0 \sin(\sigma_n\tau_n - \beta_n) = 0 \tag{45}$$

$$\omega_n a_n\beta_n' + f_0\cos(\sigma_n\tau_n - \beta_n) + \frac{1}{2}a_n \sum_{m=2}^{N} \frac{1}{4}a_m^2 (4\Gamma_{m1m1} + 2\Gamma_{mm11}) + \frac{3}{8}a_n^3\Gamma_{1111} = 0 \tag{46}$$

Substituting Eq. (45) and the steady-state motion conditions $\left(a_1' = 0 \text{ and } \gamma_1 = \sigma\tau_1 - \beta_1 = \text{constant (i.e., for } \gamma_1' = 0, \beta_1' = 0)\right)$ into Eqs. (43) and (44) yields the following modulation equations:

$$\omega_1\mu_1 a_1 = f_0 \sin\gamma_1 \tag{47}$$

$$\omega_1 a_1\sigma_1 + f_0\cos\gamma_1 + \frac{3}{8}a_1^3\Gamma_{1111} = 0 \tag{48}$$

The detuning parameter is obtained by eliminating γ from Eqs. (47) and (48). It is given as

$$\sigma_1 = -\frac{3}{8}\frac{a_1^2}{\omega_1}\Gamma_{1111} \pm \sqrt{\frac{f_0^2}{\omega_1^2 a_1^2} - \mu_1^2} \tag{49}$$

where a_1 and μ_1 are the amplitude of the complex function and damping ratio corresponding to the fundamental mode (ω_1), respectively. The right branch of the frequency-response curve is obtained when the discriminant is added while its subtraction produces the left branch.

$$\Gamma_{1111} = -\frac{1}{2}\sum_{i=1}^{2}\left[\left(\int_0^{\xi_i} {Y_{i1}}'^2 d\zeta\right)\left(\int_0^{\xi_i} {Y_{i1}}'^2 d\zeta\right)\right] = -\frac{1}{2}\left[\left(\int_0^{\xi_1} {Y_{11}}'^2 d\zeta\right)^2 + \left(\int_0^{\xi_2} {Y_{21}}'^2 d\zeta\right)^2\right]$$

6 Experimental Procedure

Figure 3 shows a schematic of the experimental setup. The experimental setup and procedure were performed according to IEEE guide [25]. The geometric and material properties of the three tested Stockbridge dampers are tabulated in Table 1. The Stockbridge damper was mounted on an electrodynamics shaker (B&K 4802). A load cell (Dytran106V1) was installed between the shaker and the fixture to measure the delivered force, and an accelerometer (B&K) was placed at the clamp to measure the acceleration of the damper. The load cell and accelerometer were connected to a dynamic signal analyzer through charge amplifiers. Signal processing and data acquisition functions were via a dynamic signal analyzer (PCI-6034E).

Using the forced response method (see IEEE guide [25]), the tests were conducted for various excitation frequencies in the range of wind-induced vibration frequencies (sweep). This frequency range was confined to frequencies greater than 10 Hz because of constraints on the shaker. The recorded frequency-response curve was then used to determine the natural frequencies. The peaks in the amplitude portion of the frequency-response function give the natural frequencies of the damper.

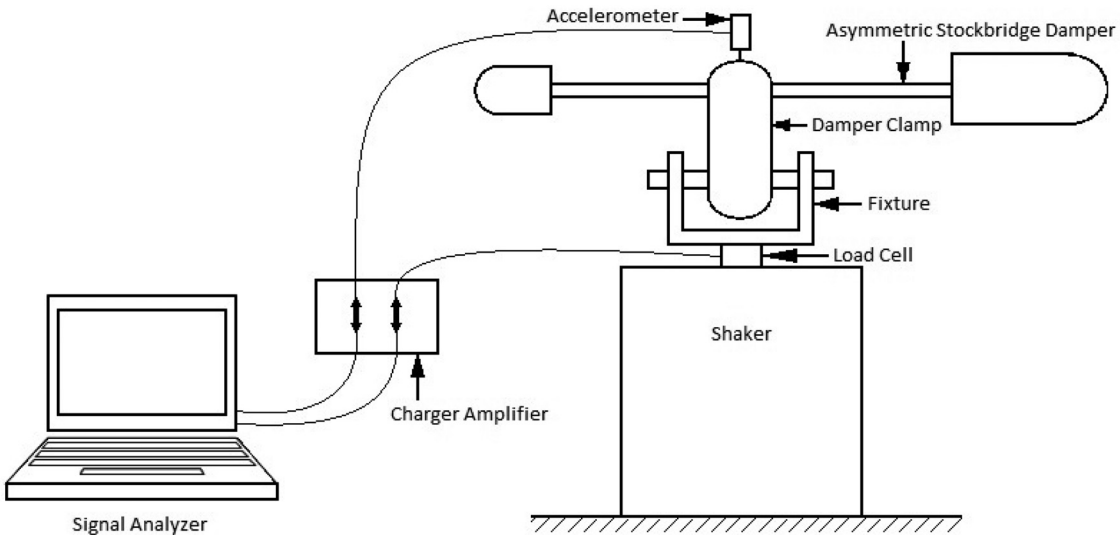

Fig. 3 Schematic of experimental setup

Table 1 Material properties and parameters

Parameter	Damper 1	Damper 2	Damper 3
m_2 (kg)	2.5	3.5	1.3
m_1 (kg)	2.5	1.5	0.7
J_1 (kg/m^2)	0.016	0.02	0.012
J_2 (kg/m^2)	0.016	0.012	0.0075
EI (N m^2	32	54.8	39.981
L_2 (m)	0.26	0.32	0.2
L_1 (m)	0.26	0.225	0.14
m (kg/m)	0.25	0.5	0.5

7 Numerical Simulations

The numerical simulations are based on the parameters listed in Table 1. The linear natural frequencies are determined by numerically solving for the roots of the frequency equation (Eq. (14)) using the bisection method in MATLAB, and the nonlinear frequencies are obtained using Eq. (35). The first five natural frequencies for each damper are tabulated in Table 2. The nonlinear frequencies show better agreement with the experimentally obtained frequencies. This is, however, dependent on the selection of the initial displacement a_0. It is noted that the symmetric damper exhibits two resonant frequencies and the asymmetric damper exhibits four.

Figures 4–6 depict the first five mode shapes of Dampers 1, 2, and 3, respectively. The left and right segment corresponds to the left- and right-hand side messenger, respectively. The figures show that the first four mode shapes of the damper are similar to the first mode shape of a cantilevered beam except that in this case there are two segments. For the damper fifth mode shape, the right-side segment corresponds to the second mode of a cantilevered beam, while the left-side segment is similar to the first mode shape.

The parameter of Damper 1 is employed in the remainder of the numerical simulations to investigate the effect of the damper mass and rotatory inertia on the resonant frequencies and response of the damper. For a given total mass ($M_1 + M_2 = 5$ kg) and total rotatory inertia 0.032 kg/m^2, the natural frequencies for various ratios of counterweight and rotatory are tabulated in Table 3. It is observed that the odd modes (i.e., first, third, and fifth) monotonically decrease with increasing ratio. The even modes (second and fourth) do not exhibit this monotony; they decrease to a certain point and then increase. In Fig. 7, the variation of the fundamental

Table 2 Analytical versus experimental natural frequencies (Hz)

Mode	Linear	Nonlinear ($a=1, k=1.0001$)	Nonlinear ($a=2, k=1.0001$)	Experimental
		Damper 1		
1	6.7023	6.9222	7.5818	—
2	30.7985	32.2457	36.5871	35.2000
3	597.9306	600.9617	610.0548	—
4	1644.3994	1648.7673	1661.8712	—
5	3222.1581	3227.2717	3242.6124	—
		Damper 2		
1	5.6414	5.7116	5.8332	—
2	13.1698	13.2439	13.4662	14.0500
3	31.0769	31.2549	31.8130	32.5000
4	52.9042	53.1911	53.9483	54.1200
5	366.6549	367.0695	367.8402	—
		Damper 3		
1	13.5152	13.8096	14.6927	15.1200
2	25.1866	25.7626	27.4907	28.1500
3	51.1492	52.0230	54.6445	55.5632
4	96.2231	97.0424	99.5003	—
5	802.2775	803.3742	806.6644	—

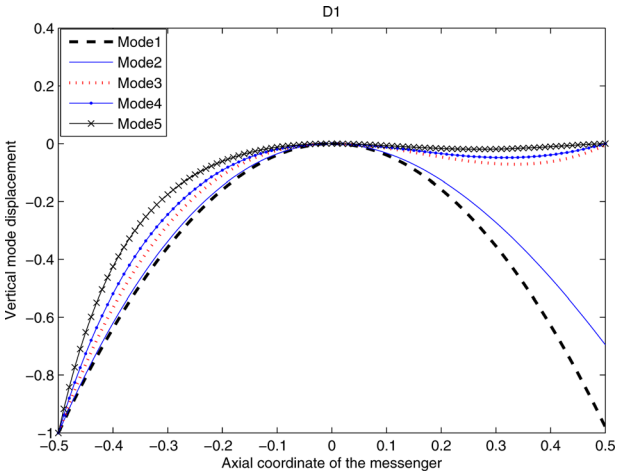

Fig. 4 Damper 1 mode shapes

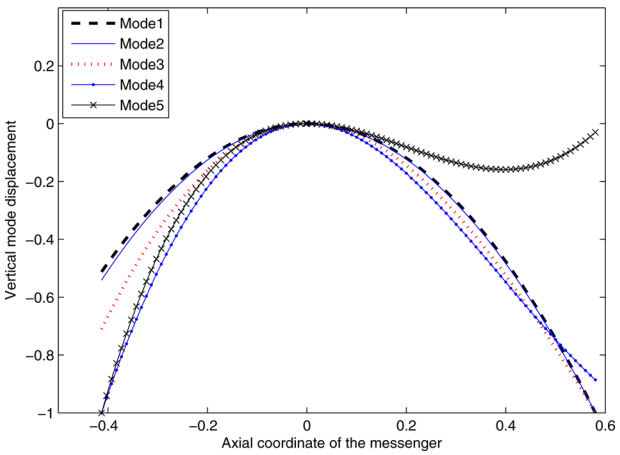

Fig. 5 Damper 2 mode shapes

nonlinear frequency with vibration amplitude is examined for various identical ratios of the counterweight mass and rotatory inertia ($M_2/M_1 = J_2/J_1$). The nonlinear frequency is observed to increase with increasing ratio of the counterweight mass and rotatory inertia. It is also observed that the nonlinear frequency increases with increasing vibration amplitude.

The frequency-response curves for the forced vibration analyses are based on Eq. (49). Because the nonlinearity is due to

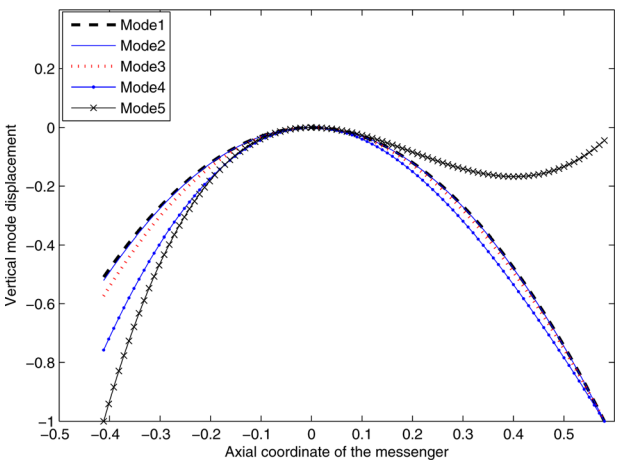

Fig. 6 Damper 3 mode shapes

Table 3 Effect of the counterweight mass and rotational inertia on natural frequencies (Hz)

m_2/m_1 J_2/J_1	Mode	Linear	Nonlinear ($a=2, k=1.0001$)
0.25	1	6.5649	6.7243
	2	8.7186	8.9210
	3	27.5317	28.2620
	4	43.9011	44.9629
	5	452.3470	453.7662
0.5	1	6.7539	6.9150
	2	7.1916	7.3599
	3	30.1661	30.9547
	4	34.0999	34.9755
	5	450.4576	451.8205
1.0	1	5.5383	5.6863
	2	8.2983	8.4888
	3	27.9550	28.6887
	4	34.7860	35.6731
	5	449.5268	450.9007
2.0	1	4.8005	4.9473
	2	10.1268	10.3636
	3	24.2538	24.8932
	4	42.4584	43.4856
	5	449.0536	450.4522
4.0	1	4.3832	4.5321
	2	13.0846	13.4066
	3	22.1385	22.7211
	4	54.7567	55.9429
	5	448.8151	450.2559

geometric stretching, it is expected that the frequency-response curve will stretch/bend to the right, which is indicative of a hardening-type nonlinearity. For a damping coefficient of $\mu_1 = 0.001$, Fig. 8 depicts the frequency-response curves for various forces ($f_0 = 1$, 0.9, and 0.8). The results in this figure indicate that the stretching of the curve and the amplitude response decrease with decreasing f_0. It is also noted that the lowest excitation amplitude ($f_0 = 0.8$) resulted in the highest asymmetrical curve from the reference point ($\sigma_1 = 0$).

In Fig. 9, the role of the damper coefficient is examined for a constant excitation amplitude ($f_0 = 1$). The frequency-response curves indicate that both vibration amplitude and the stretching decrease with increasing μ_1. This implies that damping ratio is a key parameter in ascertaining the extent of the geometric nonlinearity. The effect of the ratio of the right to left counterweight mass and rotatory inertia on the frequency-response curve is depicted in Fig. 10 for a given excitation amplitude $f_0 = 1$ and damping coefficient $\mu_1 = 0.05$. It is seen that nonlinearity stretching increases with increasing ratio and that the vibration amplitude is highest for the highest ratio.

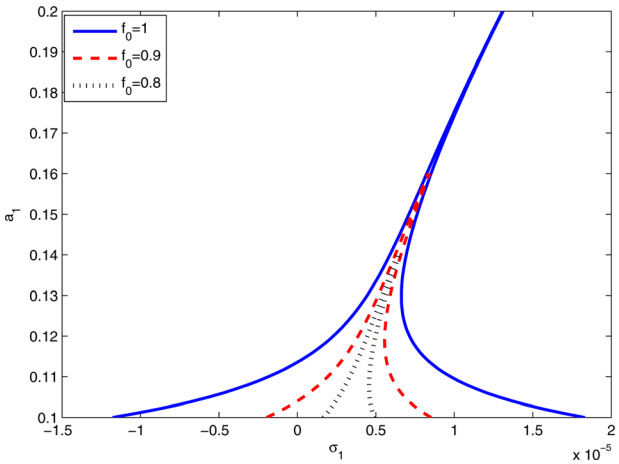

Fig. 8 Frequency-response curve for varying f_0 and constant damping

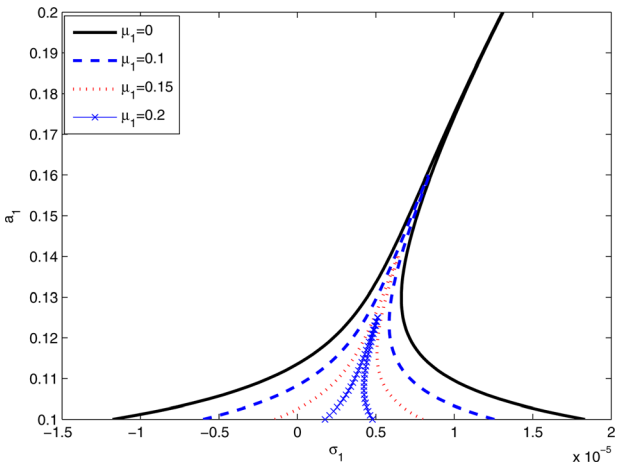

Fig. 9 Frequency-response curve for varying μ_1 and constant force

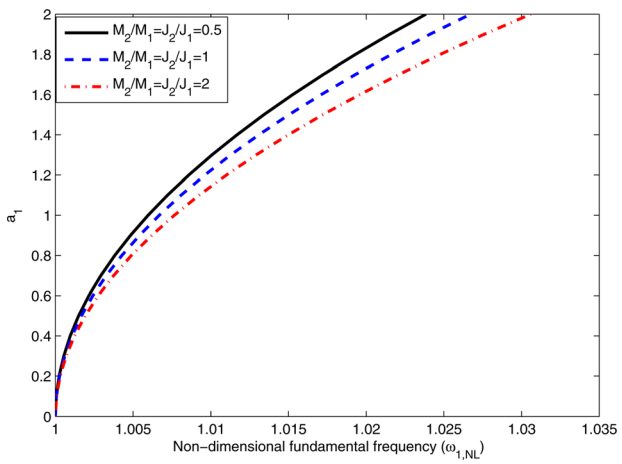

Fig. 7 Variation of fundamental nonlinear frequency with vibration amplitude

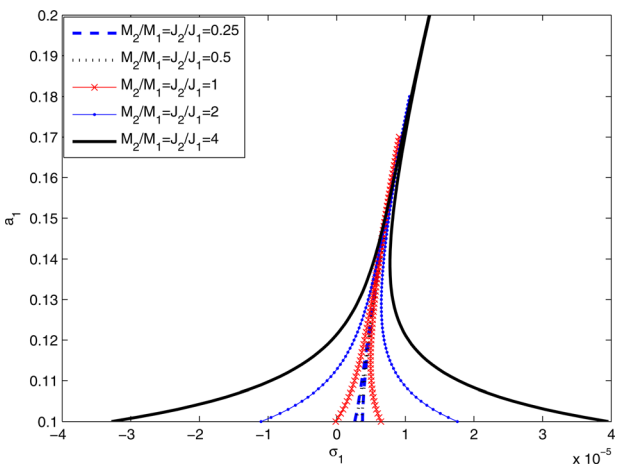

Fig. 10 Effect of the counterweight mass and rotational inertia

8 Conclusions

A nonlinear model is presented for a Stockbridge damper. The nonlinearity is due to the geometric stretching and damping coefficient of the messenger cable. The Stockbridge damper is modeled as a two cantilevered beams with tip masses. Hamilton's principle is employed to derive the equation of motion and boundary conditions. Explicit expressions are presented for the frequency equation, mode shapes, nonlinear frequency, and modulation equations. Experiments are conducted to measure the damper resonant frequencies and to validate the proposed analytical model. The proposed model is applicable to both asymmetric and symmetric Stockbridge dampers. Numerical simulations show that both the nonlinear frequency and vibration amplitude are significantly affected by the counterweight mass and rotatory inertia. It is also observed that the damping coefficient is an important factor in determining the influence of the geometric stretching of the messenger. Most importantly, the present model can be used by design engineers to predict the dynamics of Stockbridge dampers.

Acknowledgment

The financial support from Hydro One, Inc. is gratefully acknowledged.

References

[1] Chan, J., 2006, *Transmission Line Reference Book: Wind-Induced Conductor Motion*, Electrical Power Research Institute, Palo Alto, CA.

[2] Lu, M. L. C., and Chan, J. K., 2007, "An Efficient Algorithm for Aeolian Vibration of Single Conductor With Multiple Dampers," IEEE Trans. Power Delivery, **22**(3), pp. 1822–1829.

[3] Nigol, O., and Houston, H. J., 1985, "Aeolian Vibration of Single Conductor and Its Control," IEEE Trans. Power Delivery, **104**(11), pp. 3245–3254.

[4] Kraus, M., and Hagedorn, P., 1991, "Aeolian Vibration: Wind Energy Input Evaluated From Measurements on an Energized Transmission Lines," IEEE Trans. Power Delivery, **6**(3), pp. 1264–1270.

[5] Verma, H., and Hagedorn, P., 2004, "Wind Induced Vibration of Long Electrical Overhead Transmission Line Spans: A Modified Approach," J. Wind Struct., **8**(2), pp. 89–106.

[6] Rawlins, C. B., 1958, "Recent Developments in Conductor Vibration," Alcoa Technical Paper No. 13.

[7] Vecchiarelly, J., Curries, I. G., and Havard, D. G., 2000, "Computational Analysis of Aeolian Conductor Vibration With a Stockbridge-Type Damper," J. Fluids Struct., **14**(4), pp. 489–509.

[8] Havard, D. G., 1994, "Weakness in the Forced Response Method for Testing Vibration Dampers," Institute of Electrical and Electronics Engineers, San Francisco, CA, p. 664.

[9] Claren, R., and Diana, G., 1969, "Mathematical Analysis of Transmission Line Vibration," IEEE Trans. Power Delivery, **60**(2), pp. 1741–1771.

[10] Diana, G., Cigada, A., Belloli, M., and Vanali, M., 2003, "Stokbridge Type-Damper Effectiveness Evaluation: Part 1. Comparison Between Tests on Span and on the Shaker," IEEE Trans. Power Delivery, **18**(4), pp.1462–1469.

[11] Wiendl, S., Hagedorn, P., and Hochlenert, V., 2009, "Control of a Test Rig for Vibration Measurement of Overhead Transmission Lines," Proceedings of the IEEE Conference on Control and Automation, pp. 2129–2135.

[12] Wagner, H., Ramamurti, V., Sastry, R., and Hartman, K., 1973, "Dynamic of Stockbridge Dampers," J. Sound Vib., **30**(2), pp. 207–220.

[13] Barry, O., Oguamanam, D. C. D., and Lin, D. C., 2013, "Aeolian Vibration of a Single Conductor With a Stockbridge Damper," Proc. Inst. Mech. Eng., Part C, **227**(5), pp. 935–945.

[14] Barry, O., Zu, J. W., and Oguamanam, D. C. D., 2014, "Forced Vibration of Overhead Transmission Line: Analytical and Experimental Investigation," ASME J. Vib. Acoust., **136**(4), p. 041012.

[15] Barry, O., Zu, J. W., and Oguamanam, D. C. D., 2014, "Forced Vibration of Overhead Transmission Line: Analytical and Experimental Investigation," ASME J. Vib. Control, **136**(4), p. 041012.

[16] Barbieri, N., and Barbieri, R., 2012, "Dynamic Analysis of Stockbridge Damper," Adv. Acoust. Vib., **2012**(2012), p. 659398.

[17] Burgreen, D., 1951, "Free Vibrations of Pin-Ended Column With Constant Distance Between Pin-Ends," ASME J. Appl. Mech., **18**, pp. 135–139.

[18] Nayfeh, A. H., and Mook, D. T., 1979, *Nonlinear Oscillations*, Wiley, New York.

[19] Ozkaya, E., and Pakdemirli, M., 1999, "Non-Linear Vibrations of a Beam-Mass System With Both Ends Clamped," J. Sound Vib., **221**(3), pp. 491–503.

[20] Ozkaya, E., Pakdemirli, M., and Oz, H. R., 1999, "Non-Linear Vibrations of a Beam-Mass System Under Various Boundary Conditions," J. Sound Vib., **199**(4), pp. 679–696.

[21] Ozkaya, E., 2001, "Non-Linear Vibrations of a Simply-Supported Carrying Concentrated Masses," J. Sound Vib., **257**(3), pp. 413–424.

[22] Cartmell, M. P., Ziegler, S. W., Khanin, R., and Forehand, D. I. M., 2003, "Multiple Scales Analyses of the Dynamics of Weakly Nonlinear Mechanical Systems," ASME Appl. Mech. Rev., **56**(5), pp. 455–492.

[23] Pakdemirli, M., and Nayfeh, A. H., 1994, "Nonlinear Vibration of a Beam-Spring-Mass System," ASME J. Vib. Acoust., **166**(4), pp. 433–438.

[24] Nayfeh, A. H., 1981, *Introduction to Perturbation Techniques*, Wiley, New York.

[25] IEEE Committee 664, 1993, *IEEE Guide on the Measurement of the Performance of Aeolian Vibration Dampers for Single Conductors* (IEEE Std.), IEEE, pp. 664–1993.